

## Resistive switching memory properties of layer-by-layer assembled enzyme multilayers

This article has been downloaded from IOPscience. Please scroll down to see the full text article.

2012 Nanotechnology 23 155604

(<http://iopscience.iop.org/0957-4484/23/15/155604>)

View [the table of contents for this issue](#), or go to the [journal homepage](#) for more

Download details:

IP Address: 163.152.15.34

The article was downloaded on 29/03/2012 at 12:02

Please note that [terms and conditions apply](#).

# Resistive switching memory properties of layer-by-layer assembled enzyme multilayers

Hyunhee Baek<sup>1,4</sup>, Chanwoo Lee<sup>2,4</sup>, Kwang-il Lim<sup>3</sup> and Jinhan Cho<sup>1</sup>

<sup>1</sup> Department of Chemical and Biological Engineering, Korea University, Anam-dong, Seongbuk-gu, Seoul 136-713, Korea

<sup>2</sup> School of Advanced Materials Engineering, Kookmin University, Jeongneung-dong, Seongbuk-gu, Seoul 136-702, Korea

<sup>3</sup> Department of Medical and Pharmaceutical Sciences, Sookmyung Women's University, Cheongpa-ro 47-Gil 100, Yongsan-gu, Seoul 140-742, Korea

E-mail: [klim@sookmyung.ac.kr](mailto:klim@sookmyung.ac.kr) and [jinhan71@korea.ac.kr](mailto:jinhan71@korea.ac.kr)


Received 14 December 2011, in final form 3 March 2012

Published 28 March 2012

Online at [stacks.iop.org/Nano/23/155604](http://stacks.iop.org/Nano/23/155604)

## Abstract

The properties of enzymes, which can cause reversible changes in currents through redox reactions in solution, are of fundamental and practical importance in bio-electrochemical applications. These redox properties of enzymes are often associated with their charge-trap sites. Here, we demonstrate that reversible changes in resistance in dried lysozyme (LYS) films can be generated by an externally applied voltage as a result of charge trap/release. Based on such changes, LYS can be used as resistive switching active material for nonvolatile memory devices. In this study, cationic LYS and anionic poly(styrene sulfonate) (PSS) layers were alternately deposited onto Pt-coated silicon substrates using a layer-by-layer assembly method. Then, top electrodes were deposited onto the top of LYS/PSS multilayers to complete the fabrication of the memory-like device. The LYS/PSS multilayer devices exhibited typical resistive switching characteristics with an ON/OFF current ratio above  $10^2$ , a fast switching speed of 100 ns and stable performance. Furthermore, the insertion of insulating polyelectrolytes (PEs) between the respective LYS layers significantly enhanced the memory performance of the devices showing a high ON/OFF current ratio of  $\sim 10^6$  and low levels of power consumption.

 Online supplementary data available from [stacks.iop.org/Nano/23/155604/mmedia](http://stacks.iop.org/Nano/23/155604/mmedia)

(Some figures may appear in colour only in the online journal)

## 1. Introduction

The integration of enzymes with electronic elements to yield functional devices has attracted considerable attention because of the potential of these devices in applications such as biosensors and biofuel cells [1–6]. Recent research efforts have been directed toward the utilization of enzymes for the assembly of practical memory devices. For example,

it has been shown that ferritin with a large quantity of Fe ions in its inner cavity of approximately 8 nm could be converted into magnetite nanoparticles via pyrolysis of organic components. The resulting nanoparticles could be used as charge-trap elements in traditional complementary metal–oxide–semiconductor (CMOS) devices [7, 8]. Another study has showed how an electrochemical redox reaction within enzymes, monitored by cyclic voltammetry in an aqueous buffer solution, can be employed as a electric memory unit (i.e. oxidation involving charge release and

<sup>4</sup> These authors contributed equally to this work.

reduction involving charge trap). Although modifications need to be made to improve their performance and simplify their fabrication processes to the level of conventional vacuum-deposited transition-metal-oxide-coated or spin-coated organic (i.e. synthesized organometallic compounds) memory devices [9–18], these findings from bio-inspired memory devices suggest intriguing new potentials of biomaterials for use in memory devices. Our study has been motivated based on the possibility that redox reactions within enzymes in solution can be utilized for nonvolatile memory in organic devices that operate via charge-trap/release mechanisms under externally applied voltages in an air atmosphere. Furthermore, instead of using single layer structures that are prepared from spin-coating processes, we relied on intelligently designed heterogeneous film structures to enhance the memory performance of devices.

Among the various deposition methods available, the layer-by-layer (LbL) assembly method, which is based on a solution dipping process and complementary interactions (i.e. electrostatic, hydrogen-bonding and covalent-bonding interactions), has been reported to be quite useful in the preparation of organic and/or inorganic nanocomposite films that have tailored electrical properties and layer thicknesses and have various functional components on substrates with different sizes and shapes [19–30]. The Advincula group has reported that the nanometer-scale charging of LbL films, based on conjugated polymers, can provide a write–read device using current-sensing atomic force microscopy [27]. Recently, the Pal group has reported that electrostatically assembled multilayers composed of CdSe quantum dots could exhibit electrical bistability according to an externally applied voltage sweep [28]. Our group has also reported that LbL multilayer films containing gold and iron oxide nanoparticles could be employed as active layers for charge-trap flash [29] and resistive switching nonvolatile memory devices [16], respectively.

Here, we demonstrate for the first time the use of lysozyme (LYS) proteins, in which charge release and trapping take place, as resistive switching active materials in nonvolatile memory devices. In this study multilayer films composed of cationic LYS and anionic polyelectrolyte (PE) were incorporated onto Pt-coated substrates using the electrostatic LbL assembly method. We ultimately aimed to use the LbL assembly method to modulate and significantly enhance the memory performance (i.e. to obtain a high ON/OFF current ratio greater than  $\sim 10^6$  and a low level of current flow) of LYS multilayers additionally taking advantage of the additional insertion of insulating PEs of nanoscale thickness. To the best of our knowledge, the finding of nonvolatile memory functionalities of enzymes and the control of their memory performance via molecular-level manipulation of enzyme film architectures have been reported in detail for the first time in this study. We believe that our approach will be very effective for the preparation of bio-inspired memory devices, ultimately allowing easy modifications of electrical properties, low power consumption and tailored nanostructures under mild conditions (i.e. room temperature and an air atmosphere).

## 2. Materials and Methods

### 2.1. Preparation of multilayers

The concentrations of LYS (from hen egg white, Sigma Aldrich), poly(styrene sulfonate) (PSS;  $M_w = 70\,000$ , Sigma Aldrich), poly(acrylic acid) (PAA;  $M_w = 1800$ , Sigma Aldrich) and PAH ( $M_w = 70\,000$ , Sigma Aldrich) solutions used for all the experiments were  $1\text{ mg ml}^{-1}$ . The pH levels of the LYS, PAH, PSS and PAA solutions were adjusted to 6. For these experiments, LYS and PAH were used as the cationic components, and PSS and PAA were used as the anionic components. The anionic surface of the Pt-coated Si substrates was prepared via irradiation with UV light. These substrates were dipped in the cationic LYS or PAH solution for 10 min, washed twice by submersion in water for 1 min, and then air-dried with a gentle stream of nitrogen. The anionic PSS or PAA was subsequently deposited onto the LYS (or PAH)-coated substrates using the same adsorption, washing, and drying procedures described above. This process was repeated until the desired number of layers had been deposited; the resultant multilayer films were then sufficiently dried to remove the residual moisture under an air atmosphere.

### 2.2. Quartz-crystal microgravimetry (QCM) measurements

A QCM device (QCM200, SRS) was used to quantify the mass of the material deposited in each adsorption step. The resonance frequency of the QCM electrodes was about 5 MHz. The adsorbed mass of the LYS and PSS,  $\Delta m$ , can be calculated from the change in the QCM frequency,  $\Delta F$ , according to the Sauerbrey equation:  $\Delta F\text{ (Hz)} = -56.6\Delta m_A$ , where  $\Delta m_A$  is the mass change per quartz-crystal unit area in  $\mu\text{g cm}^{-2}$ . Because Kasemo and co-workers have reported that the correlation described in the Sauerbrey equation (i.e. the adsorbed mass and the frequency change) is difficult to observe when applied to viscoelastic, thick or hydrogel layers that contain water molecules in the solid–liquid interface [30], the QCM measurements in our study were made only after the adsorbed layer was sufficiently dried using nitrogen gas. In addition, the respective thicknesses of the polyelectrolytes and LYS were less than 2 nm per layer. Therefore, the polyelectrolytes/LYS multilayers that were adsorbed on the crystal surface can be regarded as rigid, but evenly distributed and thin, films that satisfy the Sauerbrey equation.

### 2.3. X-ray reflectometry

The internal structure and film thickness of LYS/PSS multilayer films were determined by x-ray reflectivity using a Cu  $K\alpha$  ( $\lambda = 1.54\text{ \AA}$ ) beam from a narrow line source of a 18 kW Rigaku Ru-300 rotating anode generator.

### 2.4. Measurement of catalytic properties of lysozymes using an Enzchek lysozyme assay kit

Fluorescence-labeled *Micrococcus lysodeikticus* cells were dissolved in a reaction buffer solution with pH of 7.5 at

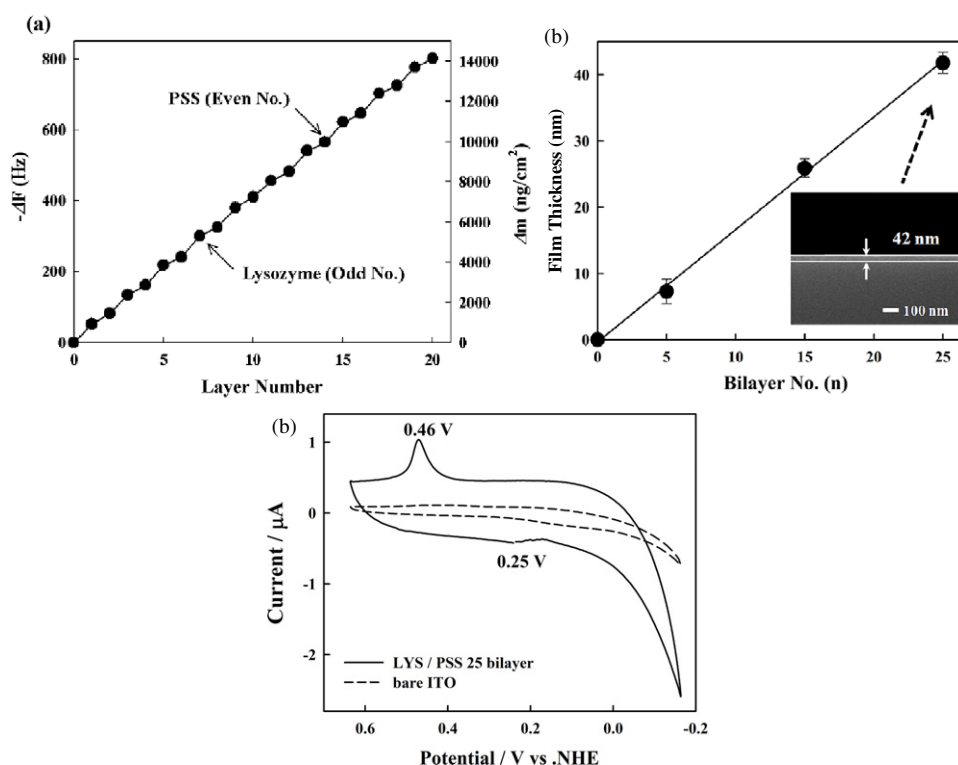


**Figure 1.** (a) QCM data of LYS/PSS multilayers as a function of the layer number. (b) Film thicknesses of (LYS/PSS)<sub>n=5,15</sub> and 25 multilayers measured from cross-sectional SEM images after drying in a vacuum. The inset is a cross-sectional SEM image of 25 bilayered films. (c) Cyclic voltammogram of a (LYS/PSS)<sub>25</sub> multilayer-coated electrode in phosphate-buffered saline (pH 7.0) with scan rate = 50 mV s<sup>-1</sup>. In this case, it was seen that in the potential region from -0.16 to 0.63 V there is an evident oxidation peak at ~0.46 V and a weak reduction peak at ~0.25 V.

a concentration of approximately 0.02 mg ml<sup>-1</sup>. In this case, the (LYS/PSS)<sub>5</sub> multilayer films were dipped into the buffer solution that contained the fluorescently labeled *M. lysodeikticus* cells, and the films were then incubated at 37 °C for 30 min. After incubation the fluorescence spectra of the reaction buffer solution were measured at an excitation wavelength ( $\lambda_{ex}$ ) of approximately 380 nm using a fluorescence spectrometer (Perkin-Elmer LS 55).

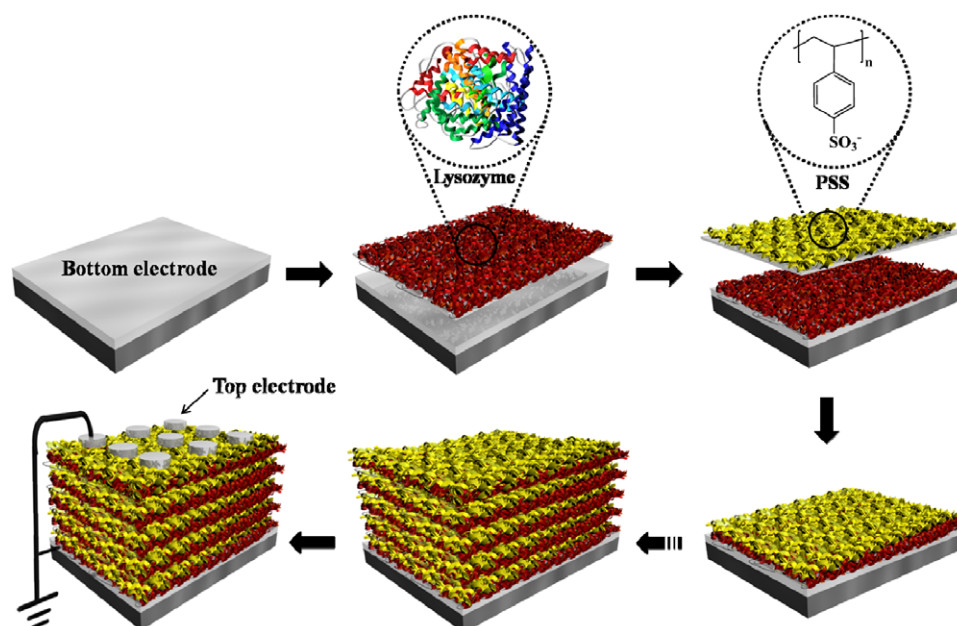
### 2.5. Fabrication of the resistive switching memory devices

All of the samples were prepared on Si substrates (2 cm × 2 cm) with a SiO<sub>2</sub> layer approximately 100 nm thick. A Ti layer, which had a thickness of 20 nm, was then deposited on the substrates, and the bottom electrode (Pt) was subsequently deposited using a DC-magnetron sputtering system. The (LYS/PSS)<sub>n</sub> multilayer films were then formed on the Pt-coated Si substrates. The top electrodes, which were 100 μm in diameter, were deposited onto the resulting nanocomposite films. To analyze the resistive switching behavior of the LbL multilayered devices, the current–voltage (*I*–*V*) curves were measured using a semiconductor parametric analyzer (SPA; Agilent 4155B) in an air environment. The dependence of the high- and low-current states on the pulsed-voltage duration was monitored using a semiconductor parametric analyzer (HP 4155A) and a pulse generator (Agilent 81104A). Although the Ag electrodes were used

as the top electrodes in these devices, similar switching behaviors were also observed when Au, Pt or tungsten top electrodes were used. This observation indicates that the Ag electrode has no distinct effect on the resistive switching characteristics of the LbL (LYS/PSS)<sub>n</sub>, (LYS/PSS/PAH/PAA)<sub>n</sub> or (LYS/PAA/PAH/PAA)<sub>n</sub> multilayers.

### 3. Results and discussion

Hen egg-white LYS is a small globular polypeptide ( $M_w \sim 14500$ ) that is composed of 129 amino acid residues, including six tryptophan and three tyrosine residues and forming up to four disulfide bonds [31]. The measured *pI* (i.e. the isoelectric point) of the LYS was approximately 11.35. Therefore, the LYS bears an overall positive charge at pH < 11.35 and a negative charge at pH > 11.35 [32]. PSS, a strong PE, is negatively charged at most pH values. On the basis of these electrostatic properties, the LbL assembly of cationic LYS and anionic PSS was performed on gold-coated substrates in deposition solution of pH 6, and the growth of the multilayers was quantitatively monitored through the use of QCM (figure 1(a)). The highly regular changes in the QCM frequency ( $-\Delta F$ ) or mass ( $\Delta m$ ) corresponding to layer number increases clearly demonstrate the LbL growth of a LYS/PSS multilayer film. Specifically, the deposition of each layer of LYS and PSS resulted in  $-\Delta F$  of  $55 \pm 4$  and  $26 \pm 2$  Hz, respectively, which correspond to  $\Delta m$  values



**Scheme 1.** Schematics for the set-up of a LYS/PSS multilayer-based nonvolatile memory device.

of  $\sim 972 \text{ ng cm}^{-2}$  and  $\sim 459 \text{ ng cm}^{-2}$ , respectively. The mass changes were calculated from the frequency changes using the Sauerbrey equation. In addition, the thicknesses of the LYS/PSS multilayers increased from approximately 8 to 42 nm when the bilayer number was increased from 5 to 25 (figure 1(b)). Furthermore, LYS/PSS multilayer films do not have a stratified (or well-ordered) structure but a mixed (or disordered) structure due to a high degree of chain interdigitation between LYS and PSS layers. This phenomenon has been demonstrated by a number of papers relating to the layer structure of LbL multilayer films [33–36]. Although we tried to investigate the layer structure of LYS/PSS multilayers using x-ray reflectivity (see supporting information, figure S1 available at [stacks.iop.org/Nano/23/155604/mmedia](http://stacks.iop.org/Nano/23/155604/mmedia)), these films exhibited only small oscillation curves originating from total film thickness without any Bragg reflection peaks caused by internal structure due to the negligible difference in electron density between organic layers (i.e. LYS and PSS layers) as well as the formation of a disordered layer structure as mentioned above.

The LYSs in the multilayers still exhibited their biological activity that breaks down bacterial cell walls by facilitating the hydrolysis of the glycosidic bonds between *N*-acetylglucosamine and *N*-acetylmuramic acid [37]. The LYS/PSS multilayer film that was dried under vacuum was dipped into a buffer solution that contained the fluorescently labeled *M. lysodeikticus* cells and then incubated at  $37^\circ\text{C}$  for 30 min. The fluorescence intensity of the buffer solution, measured at 520 nm, was 3.5 times higher than that of the buffer solution prior to incubation. These results imply that the LYS molecules inserted within the LbL multilayers maintain their inherent biological functions (see supporting information, figure S2 available at [stacks.iop.org/Nano/23/155604/mmedia](http://stacks.iop.org/Nano/23/155604/mmedia)). The electrochemical properties of the LYS/PSS multilayers were also measured using cyclic

voltammetry (CV) in a pH 7.0 phosphate buffer solution with a scan rate of  $50 \text{ mV s}^{-1}$ . As shown in figure 1(c), the CV curve for the multilayer film exhibited an oxidation peak at  $\sim +0.46 \text{ V}$  and a reduction peak at  $\sim +0.25 \text{ V}$ . The electrochemical properties of the LYS would arise from the redox reactions of multiple amino acid residues within the enzyme, such as alanine, aspartic acid, glutamic acid, tyrosine, tryptophan and cysteine [38–42]. These results suggest that the amino acid residues within the LYS/PSS multilayer films could be used as charge-trap sites for the resistive switching memory devices.

Scheme 1 depicts a nonvolatile memory device composed of LYS/PSS multilayer films deposited onto Pt-coated Si substrates and Ag electrodes with diameters of  $100 \mu\text{m}$  deposited onto the multilayer films. The electrical measurements of the nonvolatile memory cells were performed with an applied voltage in air, and Pt and Ag were used for the bottom and top electrodes, respectively. To measure the typical bipolar switching behavior (i.e. the voltage-dependent switching behavior) of the cells, initial positive voltage sweeps from 0 to  $+1.5 \text{ V}$  were applied with a limited current compliance of up to  $100 \text{ mA}$  (figure 2(a)). In this case, the current abruptly increased at  $+1.0 \text{ V}$  (which we define as  $V_{\text{SET}}$ ), which shifted the device from a highly insulating state (i.e. the ‘OFF’ state) to a low-resistance state (i.e. the ‘ON’ state). Subsequently, when the reverse voltage polarity was applied to the (LYS/PSS)<sub>25</sub> multilayer devices, the high-current state was maintained up to  $-1.3 \text{ V}$  (which we here define as  $V_{\text{RESET}}$ ), at which a sudden decrease in current took place. The OFF state was maintained from  $-1.5$  to  $+1.0 \text{ V}$ . The current ratio between the high- and low-conductivity states was greater than  $10^2$  for the proper reading voltage (e.g.  $0.1 \text{ V}$ ). Thus, sufficient margins for sensing the high- and low-resistance states were confirmed. Decreases in the number of bilayers (i.e. decreased multilayer

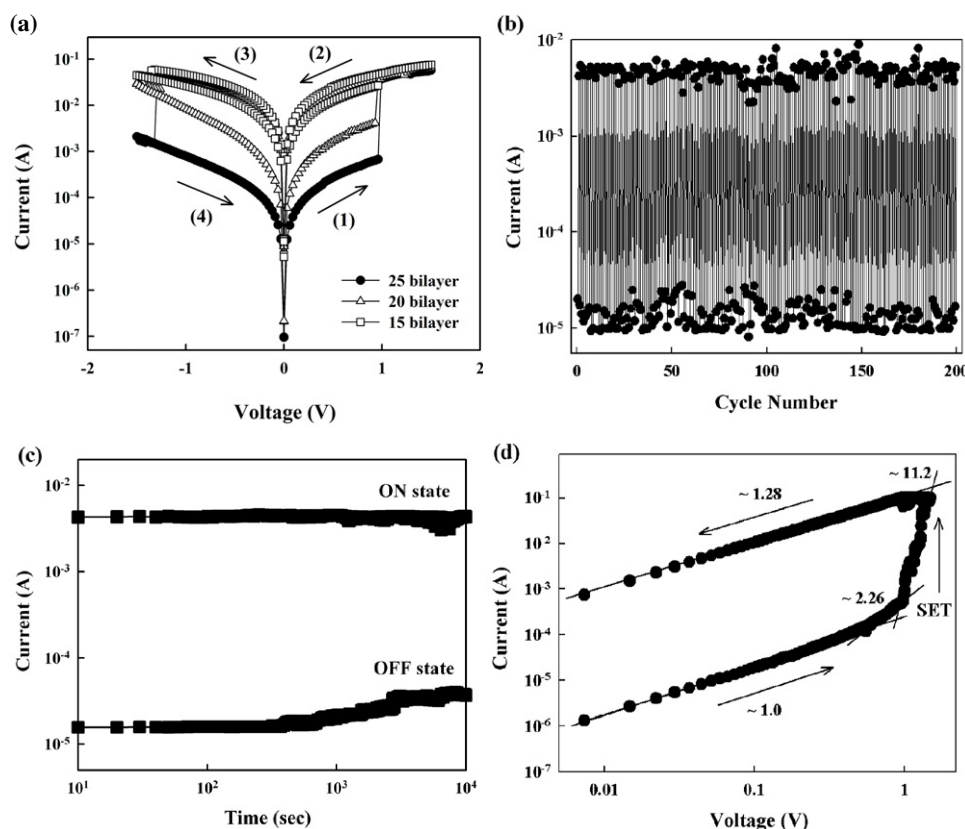


**Figure 2.** (a)  $I$ - $V$  curves of  $(\text{LYS}/\text{PSS})_n$  multilayer devices with increasing bilayer number ( $n$ ) from 5 to 25. (b) Cycling tests of 25 bilayered devices measured at a switching speed of 100 ns. (c) Retention-time test of 25 bilayered devices measured at a reading voltage of 0.1 V. (d) The linear fitting for the  $I$ - $V$  curve of 25 bilayered devices in log-log scale during the SET process in a negative voltage sweep.

thickness) led to significant increases in the OFF current level because the decreased film thickness increased the electric field. Figure 2(b) shows the results from the cycling tests that were performed with a fast switching speed of 100 ns for the 25 bilayered LYS/PSS film devices. The SET/RESET cycles have been demonstrated to withstand 200 cycles without any detectable margin deterioration. Furthermore, the retention-time tests for the  $(\text{LYS}/\text{PSS})_{25}$  multilayered devices were performed to determine their electrical stability in the ON and OFF states using a reading voltage of +0.1 V. In this experiment, a retention time of  $\sim 10^4$  s was observed for both the resistance states, and these data trends suggest that the information storage in this device is likely to persist for an even longer period of time (figure 2(c)). Recently, several reports have shown that solid electrolytes or transition-metal oxides sandwiched between an electrochemically active Ag and an inert electrode exhibited resistive switching behaviors because of an electrochemical redox reaction that involves highly mobile Ag ions [11, 43, 44]. Although Ag electrodes were used as the top electrodes in our system, similar switching behaviors were also observed with electrochemically inert top electrodes in our experiments. In particular, the  $(\text{LYS}/\text{PSS})_{25}$  multilayers sandwiched between a Pt electrode on the bottom and a tungsten (W) or Pt electrode on the top exhibited an ON/OFF current ratio greater than  $10^2$  when a reading voltage of +0.1 V was used. This observation indicates that the Ag electrode did not exert a distinct effect

on the resistive switching characteristics of the LYS/PSS multilayered devices compared to other metal electrodes even though a conductive path might be formed, in part, by metal-ion diffusion from the top electrode. In contrast, the conventional polyelectrolyte multilayers that are composed of cationic PAH and anionic PAA and do not contain charge-trap sites showed insulating characteristics without any switching memory behaviors. This result suggests that the films without charge-trap sites do not produce reversible, resistive switching behavior. Furthermore, the metal-ion diffusion of the metal electrodes into the films has no meaningful effects on the resistive switching behavior in our system. The multilayered devices displayed thermally stable memory reliability despite increasing the measurement temperature from 25 to 150 °C (see supporting information, figure S3(a) available at [stacks.iop.org/Nano/23/155604/mmedia](http://stacks.iop.org/Nano/23/155604/mmedia)). When the current curves shown in figure S3(a) of the supporting information (available at [stacks.iop.org/Nano/23/155604/mmedia](http://stacks.iop.org/Nano/23/155604/mmedia)) are replotted in  $\log R_{\text{OFF}}-\text{Temp}$  (K) and in  $\log R_{\text{ON}}-\text{Temp}$  (K),  $R_{\text{ON}}$  decreased linearly with increasing measurement temperature, indicating that conductive state is a metallic state (i.e. an Ohmic state) (see supporting information, figure S3(b) available at [stacks.iop.org/Nano/23/155604/mmedia](http://stacks.iop.org/Nano/23/155604/mmedia)). On the other hand, the temperature dependence of  $R_{\text{OFF}}$  of the devices implies a semiconducting character (see supporting information, figure S3(c) available at [stacks.iop.org/Nano/23/155604/mmedia](http://stacks.iop.org/Nano/23/155604/mmedia)).

To further clarify the conduction behavior of the LYS multilayers, the  $I$ - $V$  characteristics of the positive-voltage-sweep region of the 25 bilayered films were plotted and fitted to a double logarithmic scale (figure 2(d)). The  $I$ - $V$  relationship in the ON state clearly exhibited Ohmic conduction behavior with a slope of  $\sim 1.0$ . This relationship indicates the formation of conductive paths in the device during the SET process (i.e. switching from the low-current (OFF) to the high-current (ON) state). In contrast, the conduction behavior of the films in the OFF state was significantly more complicated. The fitting results for the high-resistance state indicate that the charge transport behavior is in agreement with a trap-controlled space charge-limited current (SCLC) model [16, 45, 46]. In the low-voltage region, the  $I$ - $V$  curve showed a linear relationship ( $I \propto V$ ), which corresponds to the Ohmic conduction mechanism based on thermally generated charge carriers. In the high-voltage region as a transition region, a quadratic dependence of the current on the voltage was predominant because all of the traps were filled with the injected carriers, which corresponds to Child's law ( $I \propto V^2$ ). This high-resistance state was changed to the low-resistance state with Ohmic conduction behavior after passing a region with a sharp increase in current flow. On the basis of these results, the different conduction behaviors in the ON and OFF states imply that the ON/OFF switching of the LYS-based memory devices is governed by the SCLC and the localized filament mechanism. The formation of the localized conductive filament paths was also confirmed using current-sensing atomic force microscopy (CS-AFM) characterization (figure 3(a)). This finding suggests that the current density between the top and the bottom electrodes is not uniform but is concentrated in the localized conduction paths, which are turned on and off during switching. This conductive filamentary path may be formed by the electron transfer between the charge-trap sites. The Murray group has reported that the electron transport in a redox polymer containing a frozen redox couple or DNA salts is caused by an electron-transfer process [47].

In general, the resistance-based nonvolatile memory effect in metal/transition-metal-oxide/metal capacitors can be explained by the memristive switching model (for bipolar switching characteristics) [10, 48] or by the filamentary conduction model (for unipolar switching characteristics) [49]. However, the bipolar switching behavior in our samples may be due to charge storage (reduced state with high resistance) and release (oxidized state with low resistance) within the charge-trap sites according to the Simmons-Verderber model (i.e. a charge-trap model) [50, 51]. In the LYS/PSS multilayered film devices, the potential redox sites in multiple residues (i.e. lysine, arginine, histidine, tyrosine, tryptophan, etc) can be used as charge-trap elements, which can considerably affect the switching mechanism. First, the positive voltage sweep from 0 to +1.0 V stores the electrons within the redox sites and induces a low-conductive state (i.e. region (1) in figure 2(a)). This OFF state is maintained until the electrons are released from the redox sites. At a SET voltage of +1.0 V (switching

from a low-current (OFF) to a high-current (ON) state), the current suddenly increased. This observation suggests that the formation of a conductive path is based on electron release from the redox sites. An increase in the external electric field to release the trapped electrons within the redox sites is thought to sharply increase the conductivity at the SET voltage (i.e.  $V_{\text{SET}} \sim +1.0$  V for the SET process). This high-conductive state (i.e. (2)  $\rightarrow$  (3)) is maintained in the reverse voltage sweep from +1.5 to -1.3 V, and the conductive path that is formed may be caused by electron hopping between the redox (or charge-trap) sites. However, the conductive paths for the electrons in the LYS multilayers are eventually broken down. This breakdown results in a decrease in conductivity that corresponds to the RESET process (i.e. switching from the ON to the OFF state).

We also confirmed the switching mechanism of the nonvolatile memory devices using the concept of charge-trap and charge-release states and Kelvin probe force microscopy (KPFM)—a technique that has been widely used to examine the changes in real-space imaging of charge-trap and charge-release states (figure 3(b)) [52–54]. The charges stored within LYSs can be detected as a change in the surface potential when the tip (i.e. a Au-coated tip of diameter 20 nm) of the KPFM instrument scans the surface of the LYS/PSS multilayers. First, a  $15 \times 15 \mu\text{m}^2$  area of the multilayer film was scanned at 10 V for charge release, and then a  $10 \times 10 \mu\text{m}^2$  area was scanned at -10 V for charge trapping. The charge-release operation was performed by scanning a  $6 \times 6 \mu\text{m}^2$  area with a +10 V bias. The relatively large scan area for KPFM measurement compared to that for CS-AFM is due to the broad surface charge distribution such as lateral diffusion in charge-trap area as well as the use of non-contact mode. Therefore, potential scans in a small area are difficult, being evidently compartmentalized into charge-trap and charge-release states because of formation of a blurred border line. As demonstrated in figure 3(b), the yellow region indicates the charge-trap state, and the dark region corresponds to the charge-release state. These results indicate that the nonvolatile devices, composed of the LYS/PSS multilayers, operate from the charge-trap/release mechanism via electron transfer between the charge-trap sites.

On the basis of these results, we attempted to significantly improve the memory performance of the LYS multilayer devices by altering the structural design using LbL assembly. Our motivation for this alteration was based on the possibility that the additional insertion of electrically insulating layers with thicknesses of approximately 2 nm between the electrically active LYS layers could effectively screen the leakage current in the ON and OFF states as shown in figure 4(a). For this attempt, (LYS/PSS/PAH/PSS)<sub>10</sub> and (LYS/PAA/PAH/poly(acrylic acid) (PAA))<sub>10</sub> multilayers were used instead of LYS/PSS multilayers as the resistive switching active film (figures 4(b) and (c)). In this case, the (LYS/PAA/PAH/PAA)<sub>10</sub> multilayer device exhibited a higher ON/OFF current ratio ( $\sim 10^6$ ) and a lower OFF current level ( $10^{-11}$  A at 0.1 V) than those (ON/OFF current ratio

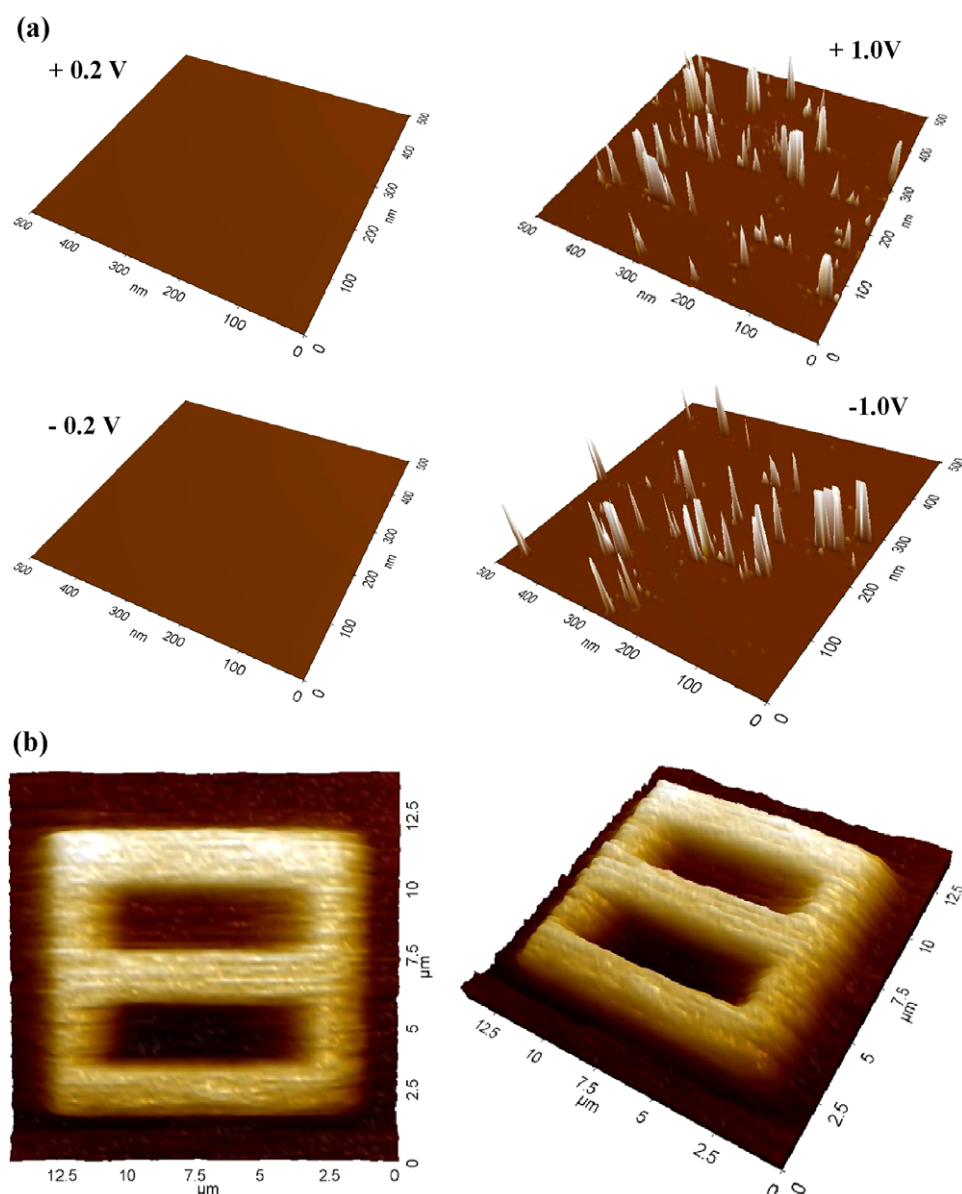


**Figure 3.** (a) CS-AFM images of (LYS/PSS)<sub>3</sub> multilayers in (a) ON and (b) OFF states, respectively. The formation of conductive filamentary paths was confirmed by current-sensing atomic force microscopy (CS-AFM) characterizations. In this case, a tungsten tip was used as a top electrode instead of a Ag electrode. The localized conductive paths were formed randomly after  $V_{\text{SET}}$  and disappeared after  $V_{\text{RESET}}$ . The formation and rupture of the randomly distributed paths were observed from ‘RESET’ and ‘SET’ processes, respectively. This suggests that the current density between the top and bottom electrode is not uniform but concentrated in these localized conducting paths, which are turned on and off during switching. The conductive filamentary path may be formed as a result of an electron hopping process. (b) Two-dimensional and three-dimensional scanning Kelvin probe force microscopy (KPFM) images of the LYS/PSS multilayered devices for charge-trap and release operation.

$\sim 10^3$  and OFF current level of  $10^{-7}$  A at 0.1 V) of the (LYS/PSS/PAH/PSS)<sub>10</sub> multilayer device. The strong sulfonic acid groups of PSS could promote electrochemical oxidation of the multilayer films, and this ‘polyanion-type doping’ would not be expected from the use of the weak carboxylic acid groups of PAA [55]. This molecular-level control over the device architecture via the use of the LbL assembly approach makes it possible to access a thickness regime and modulate the electrical properties in ways that are usually not possible with conventional processing techniques.

#### 4. Conclusions

We have demonstrated that LYS multilayers that contain no transition-metal ions have a resistive switching nonvolatile memory as a result of charge trap/release by electron transfer (or electron hopping) between the charge sites within hen egg-white lysozyme. Furthermore, we have also demonstrated that the molecular-level control over structural design could significantly enhance the electrical performance of resistive switching memory devices. We believe that our approach



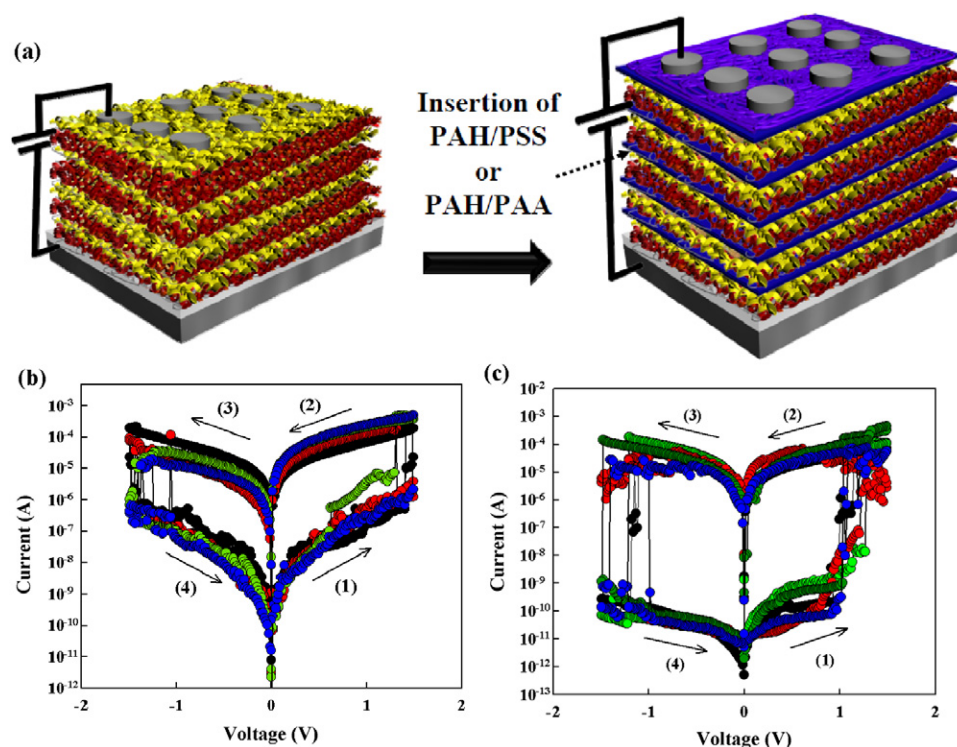


**Figure 4.** (a) Schematic for LYS-based multilayer devices containing PAH/PSS or PAH/PAA multilayers.  $I$ - $V$  curves of (a) (LYS/PSS/PAH/PSS)<sub>10</sub> and (b) (LYS/PAA/PAH/PAA)<sub>10</sub> multilayer devices.

can provide a basis for the preparation of nonvolatile memory devices with high memory performance and for the exploitation of novel resistive switching materials.

### Acknowledgments

This work was supported by the National Research Foundation (NRF) grant funded by the Korean government (MEST) (2010-0029106, 2010-0027751) and the ERC Program NRF grant funded by the Korean government (MEST) (R11-2005-048-00000-0).

### References

- [1] Nicolini C A 1998 *Biophysics of Electron Transfer and Molecular Bioelectronics* (New York: Plenum)
- [2] Hoffmann K-H 2002 *Coupling of Biological and Electronic Systems* (Berlin: Springer)
- [3] Willner I 2002 *Science* **298** 2407–8
- [4] Heller A 1990 *Acc. Chem. Res.* **23** 128–34
- [5] Yang S, Jia W-Z, Qian Q-Y, Zhou Y-G and Xia X-H 2009 *Anal. Chem.* **81** 3478–84
- [6] Li S-J, Li J, Wang K, Wang C, Xu J-J, Chen H-Y, Xia X-H and Huo Q 2010 *ACS Nano* **4** 6417–24
- [7] Miura A, Uraoka Y, Fuyuki T, Yoshii S and Yamashita I 2008 *J. Appl. Phys.* **103** 074503
- [8] Kwon M, Choi H, Chang M, Jo M, Jung S-J and Hwang H 2007 *Appl. Phys. Lett.* **90** 193512
- [9] Waser R and Aono M 2007 *Nature Mater.* **6** 833
- [10] Yang J J, Pickett M D, Li X, Ohlberg D A A, Stewart D R and Williams R S 2008 *Nature Nanotechnol.* **3** 429–33
- [11] Linn E, Rosezin R, Kugeler C and Waser R 2010 *Nature Mater.* **9** 403–6
- [12] Nagashima K, Yanagida T, Kanai M, Klamchuen A, Kim J-S, Park B H and Kawai T 2011 *Nano Lett.* **11** 2114–8
- [13] Scott J C and Bozano L D 2007 *Adv. Mater.* **19** 1452–63
- [14] Choi S, Hong S-H, Cho S H, Park S, Park S-M, Kim O and Ree M 2008 *Adv. Mater.* **20** 1766–71
- [15] Lim S L, Ling Q, Teo E Y H, Zhu C X, Chan D S H, Kang E T and Neoh K G 2007 *Chem. Mater.* **19** 5148–57
- [16] Kim Y, Lee C, Shim I, Wang D and Cho J 2010 *Adv. Mater.* **22** 5140–4
- [17] Lee C, Kim I, Shin H, Kim S and Cho J 2009 *Langmuir* **25** 11276–81
- [18] Lee C, Kim I, Choi W, Shin H and Cho J 2009 *Langmuir* **25** 4274–8
- [19] Decher G 1997 *Science* **277** 1232–7
- [20] Caruso F, Caruso R A and Möhwald H 1998 *Science* **282** 1111–4
- [21] Shiratori S S and Rubner M F 2000 *Macromolecules* **33** 4213–9
- [22] Lee B, Kim Y, Lee S, Kim Y S, Wang D and Cho J 2010 *Angew. Chem. Int. Edn* **49** 359–63
- [23] Krogman K C, Lowery J L, Zacharia N S, Rutledge G C and Hammond P T 2009 *Nature Mater.* **8** 512–8
- [24] Park J, Kim I, Shin H, Lee M J, Kim Y S, Bang J, Caruso F and Cho J 2008 *Adv. Mater.* **20** 1843–8
- [25] Podsiadlo P, Kaushik A K, Arruda E M, Waas A M, Shim B S, Xu J, Nandivada H, Pumphlin B G, Lahann J, Ramamoorthy A and Kotov N A 2007 *Science* **318** 80–3
- [26] Yoon M, Kim Y and Cho J 2010 *ACS Nano* **5** 5417–26
- [27] Jiang G, Baba A and Advincula R 2007 *Langmuir* **23** 817–25
- [28] Das B C, Batabyal S K and Pal A J 2007 *Adv. Mater.* **19** 4172–6
- [29] Lee J S, Cho J, Lee C, Kim I, Park J, Kim Y, Shin H, Lee J and Caruso F 2007 *Nat. Nanotechnol.* **2** 790–5
- [30] Höök F, Ray A, Nordén B and Kasemo B 2001 *Langmuir* **17** 8305–12
- [31] Canfield R E and Liu A K 1965 *J. Biol. Chem.* **240** 1997–2002

- [32] Scanlon M D, Jennings E and Arrigan D W M 2009 *Phys. Chem. Chem. Phys.* **11** 2272–80
- [33] Schmitt J, Gruenewald T, Decher G, Pershan P S, Kjaer K and Loesche M 1993 *Macromolecules* **26** 7058–63
- [34] Lösche M, Schmitt J, Decher G, Bouwman W G and Kjaer K 1998 *Macromolecules* **31** 8893–906
- [35] Cho J, Char K, Hong J-D and Lee K-B 2001 *Adv. Mater.* **13** 1076–8
- [36] Cho J and Char K 2004 *Langmuir* **20** 4011–5
- [37] Chakraborti S, Chatterjee T, Joshi P, Poddar A, Bhattacharyya B, Gupta S P V and Chakrabarti P 2010 *Langmuir* **26** 3506–13
- [38] Zhang L and Sun Y-G 2001 *Anal. Sci.* **17** 939–43
- [39] Zhang L and Lin X 2005 *Anal. Bioanal. Chem.* **382** 1669–77
- [40] Zhang L and Lin X 2001 *Analyst* **126** 367–70
- [41] MacDonald S M and Roscoe S G 1997 *Electrochim. Acta* **42** 1189–200
- [42] Enache T A and Oliveira-Brett A M 2011 *Bioelectrochemistry* **81** 46–52
- [43] Terabe K, Hasegawa T, Nakayama T and Aono M 2005 *Nature* **433** 47–50
- [44] Hirose Y and Hirose H 1976 *J. Appl. Phys.* **47** 2767–72
- [45] Lampert M A and Mark P 1970 *Current Injection in Solids* (New York: Academic)
- [46] Yang Y C, Pan F, Liu Q, Liu M and Zeng F 2009 *Nano Lett.* **9** 1636–43
- [47] Terrill R H, Hutchison J E and Murray R W 1997 *J. Phys. Chem. B* **101** 1535–42
- [48] Strukov D B, Snider G S, Stewart D R and Williams R S 2008 *Nature* **453** 80
- [49] Chudnovskii F A, Odynets I I, Pergament A I and Stefanovich G B 1996 *J. Solid State Chem.* **122** 95–9
- [50] Simmons J G and Verderber R R 1967 *Proc. R. Soc. A* **301** 77–102
- [51] Wang H P, Pigeon S, Izquierdo R and Martel R 2006 *Appl. Phys. Lett.* **89** 183502
- [52] Baek H, Lee C, Park J, Kim Y, Koo B, Shin H, Wang D and Cho J 2012 *J. Mater. Chem.* **22** 4645–51
- [53] Ko Y, Kim Y, Baek H and Cho J 2011 *ACS Nano* **5** 9918–26
- [54] Lee C, Kim I, Shin H, Kim S and Cho J 2010 *Nanotechnology* **21** 185704
- [55] Onitsuka O, Fou A C, Ferreira M, Hsieh B R and Rubner M F 1996 *J. Appl. Phys.* **80** 4067–71